Engineering of konjac glucomannan into respirable microparticles for delivery of antitubercular drugs

Filipa Guerreiro[a,b], Magda Swedrowska[c], Roshnee Patel[c], Noelia Flórez-Fernández[a,b,d], María Dolores Torres[d], Ana M. Rosa da Costa[e], Ben Forbes[c*] and Ana Grenha[a,b,f*]

[a]Centre for Marine Sciences (CCMar), Faculty of Sciences and Technology, Universidade do Algarve, Campus de Gambelas, 8005-139 Faro, Portugal; filiparhg@gmail.com (F. G.); noelia.florez@uvigo.es (N. F. F.); amgrenha@ualg.pt (A. G.)

[b]Centre for Biomedical Research (CBMR), Universidade do Algarve, Campus de Gambelas, 8005-139 Faro, Portugal

[c]King's College London, Institute of Pharmaceutical Science, London, SE1 9NH, UK; magda.swedrowska@kcl.ac.uk (M. S.); roshnee.patel@kcl.ac.uk (R. P.); ben.forbes@kcl.ac.uk (B. F.)

[d]Department of Chemical Engineering, University of Vigo, Faculty of Sciences, As Lagoas, 32004 Ourense, Spain; matorres@uvigo.es (M. D. T.)

[e]Algarve Chemistry Research Centre (CIQA), Faculty of Sciences and Technology, Universidade do Algarve, Campus de Gambelas, 8005-139 Faro, Portugal; amcosta@ualg.pt (A. M. R. C.)

[f]Research Institute for Medicines (iMed.ULisboa), Faculty of Pharmacy, Universidade de Lisboa, Av. Prof. Gama Pinto, 1649-003 Lisboa, Portugal

*Corresponding authors: ben.forbes@kcl.ac.uk; amgrenha@ualg.pt

Abstract

Few medically-approved excipients are available for formulation strategies to endow microcarriers with improved performance in lung drug targeting. Konjac glucomannan (KGM) is a novel, biocompatible material, comprising mannose units potentially inducing macrophage uptake for the treatment of macrophage-mediated diseases. This work investigated spray-dried KGM microparticles as inhalable carriers of model antitubercular drugs, isoniazid (INH) and rifabutin (RFB). The polymer was characterised and different polymer/drug ratios tested in the production of microparticles for which respirability was assessed *in vitro*. The swelling of KGM microparticles and release of drugs in simulated lung fluid were characterised and the biodegradability in presence of β-mannosidase, a lung hydrolase, determined. KGM microparticles were drug loaded with 66% - 91% association efficiency and had aerodynamic diameter around 3 µm, which enables deep lung penetration. The microparticles swelled upon liquid contact by 40% - 50% but underwent size reduction (> 62% in 90 min) in presence of β-mannosidase, indicating biodegradability. Finally, drug release was tested showing slower release of RFB compared with INH but complete release of both within 24 h. This work identifies KGM as a biodegradable polymer of natural origin that can be engineered to encapsulate and release drugs in respirable microparticles with physical and chemical macrophage-targeting properties.

Keywords: inhalation, konjac glucomannan, microparticles, pulmonary drug delivery

1. Introduction

In the recent decades, pulmonary drug delivery has been explored as an alternative to oral administration of drugs (Borghardt et al., 2018). When the treatment of

47 respiratory diseases by inhalation is used, a decrease in dose and administration
48 frequency is possible, minimising side effects and potentially improving both treatment
49 efficiency and patient compliance (Borghardt et al., 2018; Hadiwinoto et al., 2018). The
50 structure of the lungs is also attractive for delivery of systemically acting drugs, with a
51 large absorptive area (estimated as being approximate to 1 m^2 per kg of body weight)
52 and high permeability provided by an epithelial layer <1 μm thickness (Miranda et al.,
53 2018; Newman, 2017; Notter, 2000). Despite promising prospects, delivery of drugs to
54 the lungs remains a challenge for the developers of inhaled medicines. The
55 mechanisms of defence existing in the respiratory tract to clear the lungs of foreign
56 substances and the (in)ability of patients to use inhaler devices, are some issues
57 inherent to inhalable therapy (Newman, 2017). The development of drug carriers is
58 also challenging, as these require suitable properties to reach the desired region of the
59 lung (Hadiwinoto et al., 2018).
60 This work aimed to developing spray-dried inhalable microcarriers endowed with
61 features to target alveolar macrophages. It has been established that carriers must
62 have aerodynamic diameter < 5 μm to reach the alveolar zone (Javadzadeh and
63 Yaqoubi, 2017; Patton and Byron, 2007), while geometric sizes of 1 - 3 μm are known
64 to favour phagocytosis by alveolar macrophages (Pacheco et al., 2013). Spray-drying
65 allows microparticles to be engineered to possess these physical and performance
66 properties by optimising processing parameters. Konjac glucomannan (KGM), is a
67 polysaccharide composed by D-mannose and D-glucose units, in a 1.6-4 / 1 molar
68 ratio, 5 to 11% of which are acetylated (Devaraj et al., 2019; Guerreiro et al., 2019). It
69 was chosen as a novel matrix material for lung-targeted microcarriers due to the
70 presence of mannose units in its structure, which has been found to increase the
71 interaction between the polymer and macrophages, in a process mediated by the
72 mannose surface receptors of these cells (Du et al., 2005; Huang et al., 2015). This
73 affinity could be advantageous in the treatment of diseases involving alveolar

macrophages, such as tuberculosis, or in vaccination strategies, as dendritic cells express the same receptors. In this work, the ability of KGM to provide a matrix for microcarriers engineered to deliver drugs in the alveoli was studied. To do so, isoniazid (INH) and rifabutin (RFB), two first-line antitubercular drugs (Alves et al., 2016; Guerreiro et al., 2019), were co-loaded into KGM microparticles as model drugs. The key performance attributes of the formulations were evaluated, including their size, respirability, interaction with simulated lung conditions to release drugs and biodegradation.

2. Materials and methods

2.1. Materials

KGM and RFB were purchased from Chemos GmbH (Regenstauf, Germany). Potassium bromide (KBr; FTIR-grade), INH, glucose, mannose, hydrochloric acid (HCl), phosphate-buffered saline (PBS) pH 7.4, Gibco's Minimum Essential Medium (MEM), foetal bovine serum (FBS), L-glutamine, penicillin-streptomycin and β-mannosidase were supplied by Sigma-Aldrich (Darmstadt, Germany). Pullulan standards were purchased from PSS Polymer Standards (Mainz, Germany). Ethanol and HPLC-grade acetonitrile, methanol and potassium dihydrogen orthophosphate were supplied by Merck (Darmstadt, Germany). Di-potassium hydrogen orthophosphate was purchased from VWR (Lutterworth, UK) and Tween® 20 was obtained from Acros Organics (Geel, Belgium). Ultrapure water with 18.2 MΩ·cm residual specific resistance (Milli-Q, Millipore, UK) was used throughout the work. All other chemicals were reagent grade.

2.2. KGM hydrolysis and preparation of KGM microparticles

Commercial KGM was submitted to an acid hydrolysis to decrease the viscosity of the polymer in water, as previously reported (Guerreiro et al., 2019). KGM-based

101 microparticles were prepared from hydrolysed KGM (1.5%, w/v) dissolved in ultrapure
102 water at 70 ºC. RFB and INH were associated as model drugs to the KGM dispersion.
103 RFB was previously solubilised in 0.01 M HCl (0.75%, w/v) at room temperature and
104 added to the KGM dispersion dropwise. The KGM/RFB dispersion was stirred
105 overnight. INH was dissolved in ultrapure water at room temperature and added to the
106 previously prepared KGM/RFB dispersion. The final KGM/INH/RFB dispersion remains
107 under stirring for approximately 2 h before microparticle production. Three
108 KGM/INH/RFB dispersions, differing only in the drug content, were prepared. INH was
109 incorporated at a polymer/drug ratio of 10/1 (w/w) and 10/2 (w/w) and RFB at 10/0.5
110 (w/w) and 10/1 (w/w). The combination of different amounts of drugs and polymer
111 resulted in three KGM/INH/RFB formulations, namely 10/1/0.5 (w/w), 10/1/1 (w/w) and
112 10/2/0.5 (w/w).
113 Dry powder formulations were obtained using a Buchi B-290 laboratory mini spray-
114 dryer (Buchi Labortechnik AG, Switzerland) equipped with a high-performance cyclone.
115 The samples were spray-dried with air flow rate set at 473 L/h, aspirator at 90% and
116 the spraying dispersion at a flow rate of 0.8 mL/min. The inlet temperature was 180 ± 1
117 ºC for unloaded microparticles and 170 ± 1 ºC for drug-loaded microparticles. The yield
118 of the spray-drying process was calculated as the quotient between the resulting
119 amount of dry powder and the total amount of solids initially present in the dispersions.
120
121 2.3. KGM characterisation
122 2.3.1. NMR spectroscopy
123 Nuclear magnetic resonance (NMR) spectra of commercial and hydrolysed KGM
124 were acquired in a Bruker Avance II+ spectrometer (^{1}H: 500.13 MHz; ^{13}C: 125.77 MHz)
125 using a BBO, TXI or CP-MAS probe, at room temperature (rt). The ^{1}H NMR spectrum
126 of hydrolysed KGM was also acquired at 45 ºC. Samples were previously dissolved in
127 D_2O. ^{1}H NMR spectra were referenced to the residual internal HOD (δ 4.74 ppm). Due

to partial overlap of most signals, it was not possible to perform a proper integration. Signals attributed to mannose units are referred to as M, and those of glucose units denoted as G.

KGM: ^{1}H NMR (D_2O, 500 MHz, rt): δ_H 2.09 (s, OCOC<u>H</u>$_3$), 3.26 (br s, G-H2), 3.45-3.53 (m, M-H5), 3.53-3.58 (m, G-H5), 3.58-3.62 (m, G-H3 + G-H4), 3.68 (br s, M-H6), 3.72 (br s, M-H3), 3.78-3.86 (m, M-H4), 3.87-3.95 (m, G-H6), 4.02 (br s, M-H2), 4.42 (br s, G-H1). ^{1}H NMR (D_2O, 500 MHz, 45 ºC): δ_H 2.32 (s, OCOC<u>H</u>$_3$), 3.49 (br s, G-H2), 3.67-3.73 (m, M-H5), 3.74-3.80 (m, G-H5), 3.81-3.83 (m, G-H3 + G-H4), 3.91 (br s, M-H6), 3.94 (br s, M-H3), 4.02-4.05 (m, M-H4), 4.12-4.16 (m, G-H6), 4.24 (br s, M-H2), 4.64 (shoulder, G-H1), 4.88 (br s, M-H1). ^{13}C-NMR (D_2O, 125 MHz): δ_C 24.7 (OCO<u>C</u>H$_3$), 64.7 (G-C6+M-C6), 78.2 (C2+C3+C5+M-C4), 84.0 (G-C4), 105.3 (C1), 176.5 (O<u>C</u>OCH$_3$).

2.3.2. HPSEC analysis

KGM (commercial and hydrolysed) and unloaded KGM microparticles were analysed by High Performance Size Exclusion Chromatography (HPSEC) with a refractive index detector (Knauer K-2300, Berlin, Germany). Two columns OHpak SB-806M HQ of 300 × 8.0 mm were used in series with a 50 × 6.0 mm OHpak SB-G 6B guard column (Shodex, Tokyo, Japan). Milli-Q water (0.02% NaN_3) was used as mobile phase at 1 mL/min. The samples were dissolved in the eluent at 1 mg/mL (commercial KGM) or 5 mg/mL (hydrolysed KGM and microparticles) and filtered through a 0.45 µm filter disk (Frilabo, Maia, Portugal). A conventional calibration curve was set using pullulan standards. Method validation was performed following the procedure described in reference (Barth, 2018). The relative errors were 6% in M_w and 5% in M_n determinations.

2.3.3. Viscosity

The viscosity of commercial and hydrolysed KGM, as well as of the corresponding unloaded KGM microparticles was determined in a controlled-stress rheometer (MCR

302, Paar Physica, Austria) using a sand blasted plate-plate measuring system (0.5 mm gap, 25 mm). For this purpose, aqueous dispersions at fixed polymer content (0.5 g/L) were prepared in distilled water by stirring for 30 min at room temperature. Afterwards, samples were loaded in the rheometer measuring system, the edges were covered with paraffin oil and rested for 10 min prior to testing to enable system equilibration. The apparent viscosity flow curves (up/down) were obtained at 25 ºC following a log ramp in order to evaluate the hysteresis. Temperature was controlled by means of a Peltier system (± 0.01). All experiments were carried out at least in triplicate.

2.3.4. Oligosaccharide content

KGM (commercial and hydrolysed) and unloaded KGM microparticles were analysed by high performance liquid chromatography (HPLC) to determine the oligosaccharide composition. A preparative hydrolysis step was needed for this procedure (4% H_2SO_4, 121 °C, 20 min). Samples were dissolved and filtered through membranes (0.45 µm). Glucose and mannose oligosaccharides were used as standards. The measurements were performed on a 1100 series Hewlett-Packard chromatographer using a 300 × 7.8 mm Aminex HPX-87H column (BioRad, Hercules, CA, USA) equipped with a refractive index detector. The analysis was performed at 60 °C and the mobile phase was 0.003M H_2SO_4 (0.6 mL/min) (Flórez-Fernández et al., 2019). The limit of detection (LOD) was determined as 0.8776 µg/mL for glucose and 0.7446 µg/mL for mannose, while limits of quantification (LOQ) were 0.9444 µg/mL and 0.8040 µg/mL, respectively. The oligosaccharide content was analysed in duplicate.

2.4. Physical and morphological aspects of microparticles

The size and shape of unloaded KGM microparticles and the three formulations of KGM/INH/RFB microparticles were studied using Morphologi 4® (Malvern Instruments Limited, Malvern, UK). A small amount of dry powder was placed on the device and

dispersed on a glass plate by compressed air. The dispersed particles were analysed by a high-resolution microscope with a broad size range between 0.5 and 50 µm. The geometric diameter, circularity, elongation and convexity were calculated as the mean of 15 000 particles for each formulation.

Morphological characterisation of drug-loaded KGM microparticles was also performed by field emission scanning electron microscopy (FESEM Ultra Plus, Zeiss, Jena, Germany). Dry powders were placed onto metal plates and 5 nm thick iridium film was sputter-coated (model Q150T S/E/ES, Quorum Technologies, Lewes, UK) on the samples before viewing.

2.5. Swelling behaviour of KGM microparticles

The effect of exposing the particles to different aqueous media on the particle size was studied using unloaded KGM microparticles. Microparticle dispersions at the concentration of 10 mg/mL were prepared in PBS or simulated lung fluid (SLF). The latter is composed by 1,2-dipalmitoyl-snglycero-3-phosphocholine, 1,2-dipalmitoylsn-glycerol-3-phosphot-rac(1-glycerol) ammonium salt, cholesterol, albumin, Immunoglobulin G, transferrin, ascorbate, urate, glutathione, gentamicin and Hanks' Balanced Salt Solution and was prepared following a recently published method (Hassoun et al., 2018). The microparticle dispersions were agitated at room temperature by horizontal shaking at 300 rpm. At pre-determined times up to 90 min, samples were collected, placed on a glass slide, and particle size was analysed using the Morphologi 4®. The software was programmed to measure the size of 5000 microparticles in a scan area of 3.338 mm^2.

2.6. Evaluation of KGM microparticles biodegradation in presence of β-mannosidase

The biodegradability of KGM microparticles was evaluated by incubation of unloaded carriers in medium enriched with the enzyme β-mannosidase. The assay was performed in different media: PBS; MEM cell culture medium (supplemented with 1% v/v FBS, 1% v/v L-glutamine, 1% v/v penicillin-streptomycin); and SLF. The microparticles were incubated at a concentration of 10 mg/mL and β-mannosidase was added to the solutions at a concentration of 1.2 µg/L. The samples were incubated under horizontal shaking at 300 rpm and 37 ºC, over 90 min. At predetermined intervals, samples were collected and analysed using the Morphologi 4® as described above. Trypsin 0.25%, 0.025% or 0.0025% (v/v) was used to replace β-mannosidase to provide negative controls.

2.7. Determination of drug association efficiency and microparticle loading capacity

To determine the association efficiency (AE) of INH and RFB and the loading capacity (LC) of microparticles, each dry powder was completely solubilised in a mixture of methanol/water (60/40, v/v) under 5 min of sonication. The 10/1/0.5 (w/w) and 10/2/0.5 (w/w) formulations were solubilised at 3 mg/mL and the 10/1/1 (w/w) formulation at 2 mg/mL. After solubilisation, the samples were filtered (0.45 µm) and analysed by HPLC (Agilent 1100 series, Concord, Germany). Chromatographic separation was performed using a LiChrospher® 100 RP-18 column (4.6 µm, 4 mm ID × 250 mm, CS Chromatographie-Service GmbH, Langerwehe, Germany) equipped with a pre-column (20 x 4 mm). The injection volume was 20 µL and both drugs were detected at a wavelength of 275 nm, at room temperature. A mobile phase of 20 mM phosphate buffer (pH = 7) (A) and acetonitrile (B) was used at a flow rate of 1.0 mL/min. The elution was conducted with a gradient starting with A/B = 95%/5% (0 – 5 min), followed by transition to 30%/70% A/B ratio (5 – 8 min) and elution at the final ratio until 19 min. The retention times of INH and RFB were approximately 5 min and

20 min, respectively. Calibration curves (5 – 500 µg/mL) were obtained from INH and RFB standard solutions in methanol/water (60/40, v/v). AE and LC were calculated (n = 3) by equations (1) and (2), respectively:

AE (%) = (Actual drug content/Theoretical drug content) × 100 (1)

LC (%) = (Actual amount of drug/Weight of microparticles) × 100 (2)

2.8. *In vitro* drug deposition

The aerodynamic properties of drug-loaded KGM microparticles were analysed according to the European Pharmacopoeia (Apparatus E, European Pharmacopoeia 8.0) using the Next Generation Impactor (NGI - Copley Scientific, Nottingham, UK) equipped with an induction port. NGI has seven stages and a micro-orifice collector (MOC), which allow the separation of particles according to their aerodynamic diameter. The flow rate was calibrated at 60 L/min using a flow meter (TSI Series 4000, TSI Instruments Ltd, Buckinghamshire, UK) and the cut-off diameters ranged between 8.06 and 0.14 µm throughout the several stages. The collection plates were coated with ethanol and 1% (v/v) of Tween® 20 to prevent losses due to particle bounce. KGM/INH/RFB microparticles (30 mg) were loaded into a size 3 gelatine capsule (Meadow Laboratories Ltd, Romford, UK) and aerosolised using an RS01 device (IFR = 0.033 $kPa^{0.5}$/LPM, Plastiape, Lecco, Italy). After one actuation, the content of the capsule was discharged. The test duration time was 4 s and the content of three capsules was discharged for each experiment. A mixture of methanol/water (60/40, v/v) was used to rinse off the powder from the apparatus. Samples were sonicated for 5 min, filtered (0.45 µm) and analysed by HPLC following the analytical protocol described in section 2.7.

The quantification of drug deposited inside the impactor allows calculation of aerodynamic parameters. Mass median aerodynamic diameter (MMAD) and geometric

standard deviation (GSD) were calculated by plotting the cumulative percentage of deposited drug against the NGI stage cut-off diameters (NGI stages 1 - 7 and MOC) using a log-probability scale. Fine particle dose (FPD) was defined as the mass of drug particles with size < 5 µm. The percentage of drug released from the capsules and device was considered as the emitted dose (ED) and the fine particle fraction (FPF) was calculated as the percentage of cumulative drug mass with aerodynamic diameter lower than 5 µm.

2.9. *In vitro* drug release

To study the release profile of INH and RFB, a modified NGI was used to collect KGM/INH/RFB = 10/1/0.5 (w/w) microparticles in the second stage. The particles were emitted from three gelatine capsules and collected on a 0.45 µm nitrocellulose membrane. Each capsule was loaded with 30 mg of KGM microparticles and the flow rate was adjusted at 48 L/min. After the emission, the membranes with the deposited particles were cut and transferred to Transwell inserts. The inserts were transferred to a 6-well plate containing 5 mL of dissolution medium and kept under horizontal shaking (Mini Orbital Shaker SO5, Stuart Scientific, Staffordshire, UK) at 15 rpm and room temperature. The release profile of INH and RFB was determined on two different dissolution media, methanol/water (60/40, v/v) and SLF. At fixed time intervals, samples of dissolution medium were collected and replaced by the same volume of fresh medium. After 24 h of release, the membranes were sonicated, respectively, for 5 min when in methanol/water (60/40, v/v) and for 30 min when in SLF, to assure the total release of INH and RFB. The collected samples were analysed by HPLC as described in section 2.7. The cumulative drug release was calculated as the percentage ratio between the amount of released drug in each time interval and the total drug. The calibration curves (5–500 µg/mL) to determine the release of INH and RFB were the same obtained for the AE and LC made in methanol/water (60/40, v/v).

2.10. Statistical analysis

The t-test and one-way analysis of variance (ANOVA) with the pairwise multiple comparison procedure (Holm-Sidak method) were performed to compare two or multiple groups, respectively. All analyses were run using the GraphPad Prism® statistical program (Version 6.01) and differences were considered significant at a level of $p < 0.05$.

3. Results and discussion

3.1. KGM characterisation

3.1.1. NMR spectroscopy

The commercial and hydrolysed polymers were characterized by NMR spectroscopy. The assignment of peaks was based on reported data (Crescenzi et al., 2002). Due to its high viscosity in solution, the ^{1}H-NMR spectrum of commercial KGM was obtained from a very dilute solution and, therefore, presents a low resolution (Figure 1a). The decrease in viscosity as a consequence of hydrolysis, allowed a better resolved spectrum to be obtained for the hydrolysed polymer (Figure 1b). Both spectra were identical, with the signal of the acetyl protons at 2.09 ppm, the signal of the C-2 proton of glucose units at 3.26 ppm, the C-5 protons of mannose and glucose units at 3.49 and 3.55 ppm, respectively, the glucose C-3 and C-4 protons at 3.60 ppm, the C-6 and C-3 protons of mannose units at 3.68 and 3.72 ppm, respectively, the C-4 proton of mannose at 3.81 ppm, the C-6 protons of glucose at 3.92 ppm, the C-2 proton of mannose at 4.02 ppm, and the anomeric proton of glucose units at 4.42 ppm. The signal corresponding to the anomeric proton of mannose units was masked by the peak of HOD. However, raising the temperature to 45 ºC caused a downshift in all signals (Figure 1c), resulting in the appearance of that signal at 4.88 ppm, whilst the one of the anomeric proton of glucose appears now as a small shoulder on the solvent peak. The ^{13}C-NMR spectra (Figure 1d,e) were also identical, presenting a signal at

315 24.7 ppm attributable to the methyl carbon of acetyl groups, the signal of C-6 of
316 glucose and mannose units at 64.7 ppm, a strong and broad signal at 78.2 ppm due to
317 the C-2, C-3 and C-5 of glucose and mannose units and C-4 of the latter, with a
318 shoulder 84.0 ppm due to the C-4 of glucose, a signal 105.3 ppm corresponding to the
319 resonance of both anomeric protons, and a small signal, corresponding to the carbonyl
320 carbon of acetyl groups, at 176.5 ppm.

321 These observations were as anticipated, since the breaking of some glycosidic
322 linkages does not affect the polymer structure. Moreover, under the hydrolysis reaction
323 conditions it was not expected the hydrolysis of the acetyl groups to occur, as this
324 needs alkaline conditions (Crescenzi et al., 2002). Nevertheless, it was not possible to
325 quantify whether this occurred to a certain extent, since none of the signals of the
326 backbone protons was sufficiently separated to allow a proper integration.

327

328 **Figure 1.** ^{1}H-NMR spectra of (a) commercial and hydrolysed konjac glucomannan
329 (KGM) at (b) room temperature and (c) 45 ºC; ^{13}C CP-MAS spectra of (d) commercial
330 and (e) hydrolysed KGM. M – mannose; G – glucose; KGM – konjac glucomannan.
331 Residual solvent proton signal at *d* 4.74 ppm marked as HOD.

332

333 ### 3.1.2. Size Exclusion Chromatography

334 HPSEC was used to determine the effect of hydrolysis on the molecular weight of
335 commercial KGM and of spray-drying on that of hydrolysed KGM. The results are
336 provided in Figure 2 and Table 1. Commercial KGM was found to have a molecular
337 weight near 2 000 kDa, in line with the literature, which reports values between 200
338 and 2 000 kDa (Chua et al., 2010; Wang et al., 2015). As expected, the hydrolysed
339 polymer presented a lower molecular weight, around 700 kDa. Following hydrolysis, an
340 increase in the polydispersity index (PDI) occurred, consistent with a non-specific
341 hydrolysis reaction, in which polymer chains are randomly cut. Spray-drying had no

significant effect on the molecular weight of the polysaccharide, as can be seen in the chromatographic profiles. The small decrease in both Mw and PDI may be related to some loss of higher molecular weight chains due to either incomplete solubilization of the polymer in the preparation of solutions for spray-drying or their retention in the filtration process.

Figure 2. HPSEC chromatograms of commercial and hydrolysed konjac glucomannan (KGM), and unloaded KGM microparticles (MP).

Table 1. HPSEC analysis of commercial and hydrolysed konjac glucomannan (KGM) and unloaded KGM microparticles (MP).

Polymer	M_n (Da)*	M_w (Da)*	PDI
Commercial KGM	1 716 563	2 134 117	1.24
Hydrolysed KGM	206 787	712 413	3.45
KGM microparticles	217 241	540 644	2.49

M_n: number average molecular weight; M_w: weight average molecular weight; PDI: polydispersity index; * Relative to pullulan

3.1.3. Viscosity

The apparent viscosity of commercial and hydrolysed KGM, as well as of unloaded KGM microparticles was also determined. The results are displayed in Figure 3, where it can be clearly observed that the apparent viscosity dropped notably with increasing shear rate, all the samples exhibiting shear-thinning behaviour. This profile agrees with a typical non-entangled polymer performance in the dilute range (Torres et al., 2014).

All systems could be adequately described by the well-known power law model (R^2 > 0.990). At the lowest tested shear rates (below 1 s^{-1}), all the samples tended to common apparent viscosity values. At intermediate shear rates (between 1 and 10 s^{-1}), no important differences were observed between the apparent viscosity of the hydrolysed KGM and the unloaded KGM microparticles, whereas higher values were identified for the commercial KGM. At the highest shear rates (above 10 s^{-1}), differences were observed between the samples, according to the following order: commercial KGM > hydrolysed KGM > unloaded KGM microparticles, although the differences between the hydrolysed KGM and the unloaded KGM microparticles were small, which is consistent with the molar mass distributions obtained by HPSEC. The higher viscosity of native KGM is a natural consequence of its higher molecular weight.

Figure 3. Apparent viscosity flow curves at 25 ºC for aqueous dispersions (0.5 g/L) of konjac glucomannan (KGM; commercial and hydrolysed) and unloaded KGM microparticles (MP) prepared using hydrolysed KGM.

The observed profiles indicated a shear-thinning behaviour, which is typical of dispersions of macromolecules and suggests that, at the highest shear rates, there was an alignment of the molecules, favouring the fluid flow. Moreover, it was noteworthy that tested samples did not exhibit hysteresis loops, which represents an advantage from the point of view of processing.

3.1.4. Oligosaccharide content

KGM is a slightly branched polysaccharide composed by β-1,4-linked D-mannose and D-glucose units, typically reported to be present in a molar ratio of 1.6-4:1. Acetyl groups along the glucomannan back-bone are found, on average, every 9 to 19 sugar units. The composition can modify polymer behaviours and affect certain relevant

features, including the encapsulation efficiency and the release of drugs (Zhu, 2018), thus the impact of the hydrolysis and the spray-drying process on polymer composition was studied. The oligomer composition was determined for KGM (commercial and hydrolysed) and the unloaded KGM microparticles, the data being displayed in Table 2.

Table 2. Oligomer composition of konjac glucomannan (KGM) (commercial and hydrolysed) and spray-dried unloaded KGM microparticles (n = 2).

Sample	Oligosaccharide content		Molar ratio (mannose/glucose)
	Mannose (%)	Glucose (%)	
Commercial KGM	59.3 ± 0.8	36.7 ± 0.2	1.6
Hydrolysed KGM	63.1 ± 1.7	37.8 ± 0.6	1.7
KGM microparticles	62.1 ± 0.4	37.6 ± 0.6	1.7

All the samples exhibited similar composition. As expected, the percentage of mannose was higher than that of glucose, without significant differences between the original polymer and the processed samples. The molar ratio determined for the commercial KGM was 1.6, the same as described by several authors (Behera and Ray, 2016; Tang et al., 2018). However, the hydrolysis of the polymer slightly increased the relative amount of mannose measured with a small shift of the molar ratio from 1.6 to 1.7. Despite the decrease of molar mass and viscosity observed after the hydrolysis, the oligomeric composition was not significantly affected by the process. The molar ratio for the KGM microparticles, which were produced from the hydrolysed polymer, was unaltered compared to that of the hydrolysed polymer, indicating that spray-drying did not affect the oligomeric composition of KGM.

3.2. Preparation and characterisation of KGM microparticles

After the hydrolysis, the obtained KGM revealed to have suitable properties for processing through spray-drying. Spray-dried KGM microparticles were thus produced, associating variable amounts of INH and RFB (KGM/INH/RFB = 10/1/0.5, 10/1/1, 10/2/0.5, w/w). The drug loadings were selected to be in a similar range to other works reporting inhalation delivery of these antitubercular drugs (Gaspar et al., 2016; Rojanarat et al., 2011). The INH/RFB ratio reflects the relative potency of the drugs (Abdallah et al., 2015; Ritz et al., 2009). Moreover, the KGM proportion was kept purposely high to foster the recognition of microparticles by macrophages to improve the therapeutic outcome.

The microparticles, prepared with satisfactory yields around 80% (data not shown) (Seville et al., 2007), were characterised regarding size, shape and morphology. Parameters of size and shape measured using Morphologi 4® are provided in Table 3. The variations in theoretical drug loading had no effect on size or shape. This was expected, as the amount of drugs loaded in the microparticles was relatively small and unlikely to impact significantly on microparticle size or aspect. The geometric diameters ranged between 1.87 and 2.24 µm, which is favourable for phagocytic uptake of macrophages, an advantage when treating intracellular diseases involving these cells, such as tuberculosis (Hirota et al., 2007). Indeed, the literature reports preferential macrophage uptake of particles with sizes between 1 and 3 µm (Pacheco et al., 2013). Apart from particle size, shape is another important feature in the macrophage uptake process (Miranda et al., 2018). (Yoo and Mitragotri, 2010) have shown that spherical particles are readily internalised by macrophages whereas elongated particles may hinder phagocytosis. The KGM microparticles had high values of circularity (0.88 – 0.91) and low values of elongation (0.15 – 0.19), confirming a shape that will facilitate macrophage uptake. Additionally, the convexity of microparticles was found to reach a value of 0.99 for all formulations, which is close to the maximum value of 1. This is a

good indicator for the aerosolisation properties of KGM microparticles, as some studies demonstrate that appropriate surface convexity is critical to improve microparticle dispersion and prevent agglomeration phenomena (Du et al., 2017; Peng et al., 2016).

Table 3. Size and parameters of shape of konjac glucomannan (KGM) microparticles loaded with isoniazid (INH) and rifabutin (RFB) (mean ± SD, n = 3). Different letters mean statistically significant differences at $p < 0.05$ for each parameter.

KGM/INH/RFB (w/w)	Geometric diameter (µm)	Circularity	Elongation	Convexity
10/1/0.5	2.24 ± 2.18[a]	0.91 ± 0.14[b]	0.15 ± 0.12[c]	0.99 ± 0.04[d]
10/1/1	2.06 ± 2.15[a]	0.91 ± 0.12[b]	0.15 ± 0.12[c]	0.99 ± 0.03[d]
10/2/0.5	1.87 ± 2.11[a]	0.88 ± 0.18[b]	0.19 ± 0.16[c]	0.99 ± 0.04[d]

The size and shape of the microparticles (Table 3) were corroborated by the SEM analysis of KGM microparticles. Images of the three formulations of microparticles that were prepared in this work are shown in Figure 4, with the KGM/INH/RFB microparticles appearing as spherically-shaped particles of approximately 2 µm diameter. Despite the absence of statistically significant differences in the features between microparticle formulations (Table 3), a trend for size to decrease with the increase of the amount of associated drug was observable in the images, and mean values of geometric diameter. In parallel, the convexity also appeared more pronounced in the formulations with higher amount of drugs (KGM/INH/RFB = 10/1/1 and 10/2/0.5, w/w), which could suggest better flow properties of these formulations.

455 **Figure 4.** Representative microphotographs of konjac glucomannan (KGM)
456 microparticles associating different amounts of isoniazid (INH) and rifabutin (RFB): (a)
457 KGM/INH/RFB = 10/1/0.5 (w/w); (b) KGM/INH/RFB = 10/1/1 (w/w); (c) KGM/INH/RFB =
458 10/2/0.5 (w/w). Scale bars = 5 µm.

459

460 3.3. Swelling of KGM microparticles and biodegradability by β-mannosidase

461 KGM has a swelling capacity in water (Behera and Ray, 2016), thus, a degree of
462 swelling was expected upon contact with aqueous fluids. Unloaded KGM microparticles
463 were incubated in PBS and SLF and the evolution of their size and shape was
464 compared with the dry powder. While PBS provides a simple representation of
465 biological fluids in terms of electrolyte concentration and pH (Kyle et al., 1990), SLF
466 provides a more faithful representative of human respiratory tract lining fluid (Hassoun
467 et al., 2018; Kumar et al., 2017). The results showed that the contact with liquid media
468 had no effect on particle shape, which remained spherical (Figure 5). However, a
469 significant increase of microparticle size was observed ($p < 0.05$). The average size
470 determined for dry powder was 2.87 ± 2.34 µm (Figure 5a). Contact with either PBS or
471 SLF resulted in microparticle swelling, as observed in Figures 5b and 5c, reaching
472 average diameter of 4.34 ± 2.69 µm and 4.02 ± 1.60 µm, respectively ($p < 0.05$). These
473 correspond to average size increase of approximately 51% in PBS and 40% in SLF.
474 The particle size was monitored in short intervals over 90 min and swelling was
475 observed to occur between 20-30 min, then remained unaltered.

476

477 **Figure 5.** Unloaded KGM microparticles as observed with Morphologi4®, (a) as dry
478 powder, and after 90 min incubation in (b) phosphate buffered saline (PBS) and (c)
479 simulated lung fluid (SLF).

480

A previous study described the swelling of native KGM in a water-ethanol binary mixture, identifying three steps in the process: diffusion of water molecules into the polymer network leading to break hydrogen bonds in the loose aggregation regions; diffusion of water into the tight aggregation region, increasing chain mobility, by opening space between them, and allowing more water molecules in; hydrogen bonding between water molecules and polymeric chains (Li et al., 2009). Similar mechanisms are likely for PBS and SLF with the intermolecular hydrogen bonds of KGM breaking up in the liquid and water being absorbed into the structure of the polymer to form new hydrogen bonds. This causes expansion of the polymer chains and thus of the particles, leading to the swelling effect. The presence of salts in both fluids may further assist both the process of hydrogen bond breaking, due to increase in ionic strength, and the new hydrogen bonding, as some salts, like phosphate, have that ability (Alpert, 2018).

The swelling effect described herein is important to understand the behaviour of the carriers after reaching the deep lung and it is unclear whether this will help or hinder the interaction with macrophages. For repeat administration, it is important to evaluate conditions for the degradation of the materials used as particle matrix to avoid lung accumulation and potential toxicity. The presence of β-mannosidase in the lungs (Alkhayat et al., 1998) provides a mechanism for the degradation of KGM microparticles after deposition, by breaking the linkages between mannose units on the polysaccharide structure. Despite the description about lung expression, no information was found on the enzyme concentration in the lungs. However, it is known that the plasma concentration of β-mannosidase is 12 µg/L (“The Human Protein Atlas,” 2019). To study the biodegradability of KGM microparticles in the lungs, β-mannosidase was added to KGM microparticle dispersions in PBS, cell culture medium and SLF, at the concentration of 1.2 µg/L (Figure 6).

Figure 6. Evolution of particle size of unloaded KGM microparticles upon dispersion in PBS, cell culture medium or SLF in the presence of 1.20 µg/L β-mannosidase. Data points represent mean ± SD (n = 3; each sample ≥ 7000 particles).

In each test media, mean particle size was observed to decrease to geometric diameters around 1 µm after 90 min, corresponding to size reductions of 62% - 75%. The initial swelling of the particles may enhance the access of the enzyme to the inner particle, leading to subsequent degradation of KGM microparticles. A control study was performed replacing β-mannosidase by trypsin, a serine protease expressed in several organs in the human body, including the lung (Koshikawa et al., 1998). In this case, no reduction was observed in microparticle size, regardless of the tested concentration (0.0025% to 0.25%, w/v, data not shown).

The particle size-time profiles show the net effect of the simultaneous dynamic processes of swelling in aqueous medium and degradation upon exposure to β-mannosidase, which have opposing effects, with the size reducing action of enzymatic activity dominating. These data provide an indication of the potential for biodegradation of KGM microparticles upon pulmonary delivery, which is reported for the first time herein and is favourable for the application. Further development of the KGM microparticle excipient platform should include detailed investigation of particle disintegration and polymer breakdown in more biorelevant models of the metabolic environment in the lungs (Enlo-Scott et al., 2021) and studies to attain a mechanistic understanding of how these processes affect drug release.

3.4. Evaluation of drug association efficiency and microparticle loading capacity

INH and RFB were associated with KGM microparticles as model antibiotics. As depicted in Table 4, both drugs were successfully incorporated into the microparticles,

535 although the association of INH was significantly higher than that of RFB in the three
536 formulations ($p < 0.05$).
537
538 **Table 4.** Association efficiency (AE) and loading capacity (LC) of isoniazid (INH) and
539 rifabutin (RFB) in different konjac glucomannan (KGM)-based microparticles (mean ±
540 SD, n = 6). Different letters mean statistically significant differences at $p < 0.05$ for each
541 parameter.

KGM/INH/RFB (w/w)	Drug	Association efficiency (%)	Loading capacity (%)
10/1/0.5	INH	90.5 ± 3.4[a]	7.5 ± 0.3[f]
	RFB	73.6 ± 8.6[d]	2.9 ± 0.3[h]
10/1/1	INH	84.5 ± 4.9[b]	7.0 ± 0.4[f]
	RFB	73.3 ± 1.8[d]	6.1 ± 0.2[i]
10/2/0.5	INH	78.1 ± 3.5[c]	13.0 ± 0.6[g]
	RFB	65.9 ± 2.6[e]	2.6 ± 0.1[j]

542
543
544 INH association values ranged between 78% and 91%, although an increase of
545 theoretical drug loading in the microparticles significantly decreased the proportion of
546 INH that was loaded ($p < 0.05$). RFB presented a different behaviour, with association
547 efficiency ranging between 66% and 74%. An increase in the amount of RFB in the
548 formulation, from KGM/INH/RFB = 10/1/0.5 to 10/1/1 (w/w), did not produce any
549 alteration on drug association, which remained around 73% - 74%. However, the
550 association of RFB was lower for the formulation 10/2/0.5 (w/w), registering 66% ($p <$
551 0.05). The values for the loading capacity ranged within approximately 7% - 13% and

552 3% - 6%, for INH and RFB, respectively. Naturally, INH showed higher loading than
553 RFB ($p < 0.05$), mirroring the theoretical loadings. Moreover, INH and RFB loadings
554 were found to be lower than the theoretical loadings, which were 9.1%/3.7%,
555 8.5%/7.3%, 15.6%/3.3% for the formulations 10/1/0.5 (w/w), 10/1/1 (w/w) and 10/2/0.5
556 (w/w), respectively.
557
558 3.5. Aerodynamic characterisation of KGM microparticles
559 Characterising the aerosolisation properties of KGM/INH/RFB microparticles is
560 crucial to establish the potential of the system for inhalable applications. The
561 microparticle formulations were evaluated using a cascade impactor (NGI) and their
562 aerodynamic properties are shown in Table 5.
563 The emitted dose for all formulations was above 91% indicating good dispersibility of
564 the KGM-based microparticles regardless of some statistically significant differences ($p
565 < 0.05$) between certain formulations with different proportions of INH and RFB. A
566 MMAD around 3 µm was obtained for all three formulations, along with FPF of 55% -
567 60%. The latter indicates the fraction of microparticles with aerodynamic diameter
568 below 5 µm, thus having suitable properties to reach the respiratory zone of the lungs
569 (Patton and Byron, 2007). GSD values of 2.5 – 3 µm were determined, suggesting high
570 polydispersity of dry powders, which is coincident with SEM microphotographs.
571 An initial evaluation of KGM microparticles identified their potential theoretical
572 suitability for inhalation purposes, although an experimental determination of particle
573 aerodynamics was not performed (Guerreiro et al., 2019). The present work
574 demonstrates that, as a whole, KGM microparticles possess suitable properties for
575 deep lung delivery. The morphology of the particles contributes positively to this effect
576 as the convexity, previously described in section 3.2, improves the dispersibility of the
577 particles for inhalation to the deeper zones of the lungs (Du et al., 2017; Peng et al.,
578 2016).

579 **Table 5.** Aerodynamic parameters of konjac glucomannan (KGM) microparticles loaded with isoniazid (INH) and rifabutin (RFB) (mean ± SD, n

580 = 6). Different letters mean statistically significant differences at $p < 0.05$ for each parameter.

KGM/INH/RFB (w/w)	Drug	Emitted dose (%)	MMAD (µm)	GSD (µm)	FPD <5 µm (mg)	FPF <5 µm (%)
10/1/0.5	INH	91.8 ± 1.2^{a}	2. 89± 0.16^{d}	2.70 ± 0.12^{f}	2.71 ± 0.16^{l}	54.7 ± 2.3^{p}
	RFB	96.6 ± 1.9^{c}	3.02 ± 0.17^{e}	2.82 ± 0.09^{i}	1.40 ± 0.11^{n}	56.5 ± 2.9^{r}
10/1/1	INH	94.5 ± 1.8^{b}	3.05 ± 0.05^{d}	2.89 ± 0.10^{g}	2.64 ± 0.11^{l}	59.0 ± 1.9^{q}
	RFB	97.5 ± 1.3^{c}	3.24 ± 0.09^{e}	2.93 ± 0.10^{j}	2.62 ± 0.22^{o}	59.9 ± 1.4^{s}
10/2/0.5	INH	91.7 ± 1.3^{a}	3.05 ± 0.16^{d}	2.47 ± 0.19^{h}	5.24 ± 0.23^{m}	57.2 ± 1.8^{q}
	RFB	95.7 ± 1.6^{c}	3.17 ± 0.15^{e}	2.53 ± 0.13^{k}	1.26 ± 0.17^{n}	57.8 ± 1.6^{s}

581 FPD: fine particle dose; FPF: fine particle fraction; GSD: geometric standard deviation; MMAD: mass median aerodynamic diameter

582 The deposition profile of INH and RFB across the different stages of the NGI aerosolisation
583 (Figure 7) can be analysed further. The first observation to highlight is that the deposition of INH
584 and RFB was generally similar for all formulations of microparticles, which indicates a
585 homogeneous distribution of the drugs and is consistent with the delivery of co-association
586 drugs. Moreover, a similar deposition profile was observed for the three formulations of KGM
587 microparticles. Although not reaching statistical significance, the deposition of the drugs in the
588 stages of the NGI representing the deeper zones of the lung (stages 5 to MOC) was slightly
589 higher in the microparticles KGM/INH/RFB = 10/1/1 (w/w) (23%) comparing with the other two
590 formulations, which obtained 20% (KGM/INH/RFB = 10/1/0.5, w/w) and 18% (KGM/INH/RFB =
591 10/2/0.5, w/w). This means that the former may have a greater propensity to deposit powder in
592 the lower airways, and is reflected in a higher FPF (Table 5) which is derived from the impactor
593 data.
594
595 **Figure 7.** *In vitro* aerodynamic deposition of isoniazid (INH) and rifabutin (RFB) in the Next
596 Generation Impactor (NGI) after aerosolisation of drug-loaded konjac glucomannan (KGM)
597 microparticles: (a) KGM/INH/RFB = 10/1/0.5 (w/w); (b) KGM/INH/RFB =10/1/1 (w/w); (c)
598 KGM/INH/RFB =10/2/0.5 (w/w). Values are mean ± SD, n = 6. MOC: micro-orifice collector.
599 Statistical significance is indicated with *($p < 0.05$).
600
601 3.6. *In vitro* drug release
602 The *in vitro* release of INH and RFB was studied in two different release media,
603 methanol/water (60/40, v/v) and SLF. Methanol/water medium was previously used to determine
604 drug association efficiency, by releasing 100% INH and RFB. SLF is representative of the
605 human respiratory tract lining fluid and can be used in *in vitro* studies, such as those
606 determining the solubility of inhaled drugs, the dissolution of aerosol particles and particle-lung

607 cell interactions (Hassoun et al., 2018; Kumar et al., 2017). The release profiles were
608 determined for a representative microparticle formulation, KGM/INH/RFB 10/1/0.5 (w/w). INH
609 exhibited a similar release profile in methanol/water and SLF (Figure 8a) with only small
610 statistically significant differences observed at initial time points (up to 15 min, $p < 0.05$) and
611 profiles that largely overlap. Approximately 50% of the drug was released in 10 min
612 (methanol/water) and 45 min (SLF), showing a faster release in methanol/water than in SLF.
613 After 12 h, the released antibiotic reached 84% in both dissolution media, while 96% - 97% of
614 the drug was released in 24 h.

615 The release of RFB in methanol/water (Figure 8b) was found to be very similar to that of INH,
616 no significant differences being observed. After 15 min, 50% of the drug was released. In turn,
617 the release was much more sustained in SLF ($p < 0.05$); instead of a rapid initial release, only
618 9% of RFB was released after 15 min. Shortly after 3 h, the release rates became similar in both
619 media. At 12 h, the released RFB was 82% and 90% in methanol/water and SLF, respectively,
620 reaching 94% - 99% at 24 h. The release of RFB was expected to be generally slower than that
621 of INH. This is because RFB is hydrophobic and is a larger molecule (847.02 g/mol *versus*
622 137.14 g/mol for INH) (Magee et al., 1996; Razak et al., 2014). However, the release in
623 methanol/water revealed a similar behaviour, possibly because these solvents provide a good
624 and rapid dissolution of the carrier matrix, composed of KGM, and high solubility of RFB in the
625 release medium due to the methanol content (Pfizer Canada Inc., 2015). A preliminary
626 evaluation performed during this study has shown that SLF is less solubilising as a dissolution
627 medium for RFB comparing with methanol/water (26 µg/mL and 185 µg/mL, respectively).
628
629 **Figure 8.** *In vitro* release profile of (a) isoniazid (INH) and (b) rifabutin (RFB) from
630 KGM/INH/RFB = 10/1/0.5 (w/w) microparticles in methanol (MeOH)/water (H_2O) and simulated
631 lung fluid (SLF). Graphics with expanded representation of release profiles at initial time points

were inserted. Data represented as mean ± SD (n ≥ 3). Statistical significance is indicated as * ($p < 0.05$).

Drug release of the same particles in PBS pH 7.4 containing 1% (v/v) Tween 80® (Guerreiro et al., 2019) found a faster release of both drugs, although the methodology was different, with microparticles being submerged in the release medium, which confounds a direct comparison.

4. Conclusion

This work describes the development of an inhalable therapy using KGM as carrier matrix material. First the physical and chemical properties of KGM as a polymer were determined to define polymer size, structure and unit composition. Thus characterised, KGM was successfully spray-dried to form microparticles loaded with model drug combinations of isoniazid and rifabutin and exhibited suitable characteristics for delivery to the lungs by inhalation. The aerodynamic diameter was around 3 µm, which is ideal for KGM microparticles to reach the alveolar region. Moreover, the geometric diameter of 2 µm, spherical shape and presence of mannose units as part of the microparticle composition fit the target product profile for improved interaction with the alveolar macrophages. Preliminary studies show the potential for biodegradation of KGM microparticles in the lung environment which is necessary for safety. Drug release was characterised in simulated lung fluid with both drugs showing biphasic profile with faster release of 60% of drug, followed by a slower release of the drug load within 24 h. Comparison of formulations with different levels of drug-loading revealed similar aerodynamic behaviours and formulation characteristics. These promising attributes of KGM microparticles encourage their continued development as a carrier to enhance lung delivery of antitubercular drugs.

Acknowledgments

This work was supported by National Portuguese funding through FCT - Fundação para a Ciência e a Tecnologia, through projects PTDC/DTP-FTO/0094/2012, UIDB/04326/2020 and the PhD scholarship to Filipa Guerreiro (SFRH/BD/115628/2016). The support of Maria João Ferreira, from the Association of Instituto Superior Técnico for Research and Development (IST-ID), in NMR spectra acquisition, is highly acknowledged.

References

Abdallah, A.M., Hill-Cawthorne, G.A., Otto, T.D., Coll, F., Guerra-Assunção, J.A., Gao, G., Naeem, R., Ansari, H., Malas, T.B., Adroub, S.A., Verboom, T., Ummels, R., Zhang, H., Panigrahi, A.K., McNerney, R., Brosch, R., Clark, T.G., Behr, M.A., Bitter, W., Pain, A., 2015. Genomic expression catalogue of a global collection of BCG vaccine strains show evidence for highly diverged metabolic and cell-wall adaptations. Sci. Rep. 5, 1–15.

Alkhayat, A.H., Kraemer, S.A., Leipprandt, J.R., Macek, M., Kleijer, W.J., Friderici, K.H., 1998. Human beta-mannosidase cDNA characterization and first identification of a mutation associated with human beta-mannosidosis. Hum. Mol. Genet. 7, 75–83.

Alpert, A.J., 2018. Effect of salts on retention in hydrophilic interaction chromatography. J. Chromatogr. A 1538, 45–53.

Alves, A., Cavaco, J., Guerreiro, F., Lourenço, J., Rosa da Costa, A., Grenha, A., 2016. Inhalable Antitubercular Therapy Mediated by Locust Bean Gum Microparticles. Molecules 21, 702.

Barth, H.G., 2018. Accuracy validation of size-exclusion chromatography. LCGC North Am. 36, 142–145.

680 Behera, S.S., Ray, R.C., 2016. Konjac glucomannan, a promising polysaccharide of
681 Amorphophallus konjac K. Koch in health care. Int. J. Biol. Macromol. 92, 942–956.

682 Borghardt, J.M., Kloft, C., Sharma, A., 2018. Inhaled Therapy in Respiratory Disease: The
683 Complex Interplay of Pulmonary Kinetic Processes. Can. Respir. J. 2018, 1–11.

684 Chua, M., Baldwin, T.C., Hocking, T.J., Chan, K., 2010. Traditional uses and potential health
685 benefits of Amorphophallus konjac K. Koch ex N.E.Br. J. Ethnopharmacol. 128, 268–278.

686 Crescenzi, V., Skjåk-Bræk, G., Dentini, M., Masci, G., Bermalda, M.S., Risica, D., Capitani, D.,
687 Mannina, L., Segre, A.L., 2002. A high field NMR study of the products ensuing from
688 Konjak glucomannan C(6)-oxidation followed by enzymatic c(5)-epiderization.
689 Biomacromolecules 3, 1343–1352.

690 Devaraj, R.D., Reddy, C.K., Xu, B., 2019. Health-promoting effects of konjac glucomannan and
691 its practical applications: A critical review. Int. J. Biol. Macromol. 126, 273–281.

692 Du, J., Sun, R., Zhang, S., Zhang, L.-F., Xiong, C.-D., Peng, Y.-X., 2005. Novel polyelectrolyte
693 carboxymethyl konjac glucomannan-chitosan nanoparticles for drug delivery. I.
694 Physicochemical characterization of the carboxymethyl konjac glucomannan-chitosan
695 nanoparticles. Biopolymers 78, 1–8.

696 Du, P., Du, J., Smyth, H.D.C., 2017. Evaluation of Granulated Lactose as a Carrier for Dry
697 Powder Inhaler Formulations 2: Effect of Drugs and Drug Loading. J. Pharm. Sci. 106,
698 366–376.

699 Enlo-Scott, Z., Bäckström, E., Mudway, I., Forbes, B., 2021. Drug metabolism in the lungs:
700 opportunities for optimising inhaled medicines. Expert Opin. Drug Metab. Toxicol.

701 Flórez-Fernández, N., Domínguez, H., Torres, M.D., 2019. Advances in the biorefinery of

Sargassum muticum: Valorisation of the alginate fractions. Ind. Crops Prod. 138, 111483.

Gaspar, D.P., Faria, V., Gonçalves, L.M.D., Taboada, P., Remuñán-López, C., Almeida, A.J., 2016. Rifabutin-loaded solid lipid nanoparticles for inhaled antitubercular therapy: Physicochemical and in vitro studies. Int. J. Pharm. 497, 199–209.

Guerreiro, F., Pontes, J.F., Rosa da Costa, A.M., Grenha, A., 2019. Spray-drying of konjac glucomannan to produce microparticles for an application as antitubercular drug carriers. Powder Technol. 342.

Hadiwinoto, G.D., Kwok, P.C.L., Lakerveld, R., 2018. A review on recent technologies for the manufacture of pulmonary drugs. Ther. Deliv. 9, 47–70.

Hassoun, M., Royall, P.G., Parry, M., Harvey, R.D., Forbes, B., 2018. Design and development of a biorelevant simulated human lung fluid. J. Drug Deliv. Sci. Technol. 47, 485–491.

Hirota, K., Hasegawa, T., Hinata, H., Ito, F., Inagawa, H., Kochi, C., Soma, G.I., Makino, K., Terada, H., 2007. Optimum conditions for efficient phagocytosis of rifampicin-loaded PLGA microspheres by alveolar macrophages. J. Control. Release 119, 69–76.

Huang, Z., Gan, J., Jia, L., Guo, G., Wang, C., Zang, Y., Ding, Z., Chen, J., Zhang, J., Dong, L., 2015. An orally administrated nucleotide-delivery vehicle targeting colonic macrophages for the treatment of inflammatory bowel disease. Biomaterials 48, 26–36.

Javadzadeh, Y., Yaqoubi, S., 2017. Therapeutic nanostructures for pulmonary drug delivery, in: Nanostructures for Drug Delivery. Elsevier Inc., pp. 619–638.

Koshikawa, N., Hasegawa, S., Nagashima, Y., Mitsuhashi, K., Tsubota, Y., Miyata, S., Miyagi, Y., Yasumitsu, H., Miyazaki, K., 1998. Expression of trypsin by epithelial cells of various tissues, leukocytes, and neurons in human and mouse. Am. J. Pathol. 153, 937–944.

Kumar, A., Terakosolphan, W., Hassoun, M., Vandera, K.K., Novicky, A., Harvey, R., Royall, P.G., Bicer, E.M., Eriksson, J., Edwards, K., Valkenborg, D., Nelissen, I., Hassall, D., Mudway, I.S., Forbes, B., 2017. A Biocompatible Synthetic Lung Fluid Based on Human Respiratory Tract Lining Fluid Composition. Pharm. Res. 34, 2454–2465.

Kyle, H., Ward, J.P.T., Widdicombe, J.G., 1990. Control of pH of airway surface liquid of the ferret trachea in vitro. J. Appl. Physiol. 68, 135–140.

Li, L., Ruan, H., Ma, L.L., Wang, W., Zhou, P., He, G.Q., 2009. Study on swelling model and thermodynamic structure of native konjac glucomannan. J. Zhejiang Univ. Sci. B 10, 273–279.

Magee, K.P., Wimberley, D., Crane, G., Sobhi, S., Bawdon, R.E., 1996. Ex Vivo Human Placental Transfer of Rifampin and Rifabutin. Infect. Dis. Obstet. Gynecol. 4, 319–322.

Miranda, M.S., Rodrigues, M.T., Domingues, R.M.A., Torrado, E., Reis, R.L., Pedrosa, J., Gomes, M.E., 2018. Exploring inhalable polymeric dry powders for anti-tuberculosis drug delivery. Mater. Sci. Eng. C 93, 1090–1103.

Newman, S.P., 2017. Drug delivery to the lungs: Challenges and opportunities. Ther. Deliv. 8, 647–661.

Notter, R.H., 2000. Discovery of endogenous lung surfactant and overview of its metabolism and actions, in: Lung Surfactants: Basic Science and Clinical Applications. pp. 119–149.

Pacheco, P., White, D., Sulchek, T., 2013. Effects of Microparticle Size and Fc Density on Macrophage Phagocytosis. PLoS One 8, e60989.

Patton, J.S., Byron, P.R., 2007. Inhaling medicines: Delivering drugs to the body through the lungs. Nat. Rev. Drug Discov. 6, 67–74.

746 Peng, T., Lin, S., Niu, B., Wang, X., Huang, Y., Zhang, X., Li, G., Pan, X., Wu, C., 2016.
747 Influence of physical properties of carrier on the performance of dry powder inhalers. Acta
748 Pharm. Sin. B 6, 308–318.

749 Pfizer Canada Inc., 2015. Mycobutin, Pfizer Canada Inc. Pfizer Canada Inc., Kirkland.

750 Razak, S.A., Fariq, S., Syed, F., Abdullah, J.M., Adnan, R., 2014. Characterization , phase
751 solubility studies and molecular modeling of Isoniazid and its β -Cyclodextrin complexes. J.
752 Chem. Pharm. Res. 6, 291–299.

753 Ritz, N., Tebruegge, M., Connell, T.G., Sievers, A., Robins-Browne, R., Curtis, N., 2009.
754 Susceptibility of Mycobacterium bovis BCG vaccine strains to antituberculous antibiotics.
755 Antimicrob. Agents Chemother. 53, 316–318.

756 Rojanarat, W., Changsan, N., Tawithong, E., Pinsuwan, S., Chan, H.K., Srichana, T., 2011.
757 Isoniazid proliposome powders for inhalation-preparation, characterization and cell culture
758 studies. Int. J. Mol. Sci. 12, 4414–4434.

759 Seville, P.C., Learoyd, T.P., Li, H.Y., Williamson, I.J., Birchall, J.C., 2007. Amino acid-modified
760 spray-dried powders with enhanced aerosolisation properties for pulmonary drug delivery.
761 Powder Technol. 178, 40–50.

762 Tang, J., Chen, J., Guo, J., Wei, Q., Fan, H., 2018. Construction and evaluation of fibrillar
763 composite hydrogel of collagen/konjac glucomannan for potential biomedical applications.
764 Regen. Biomater. 5, 239–250.

765 The Human Protein Atlas [WWW Document], 2019. . MANBA. URL
766 https://www.proteinatlas.org/ENSG00000109323-MANBA/blood (accessed 11.4.19).

767 Torres, M.D., Hallmark, B., Wilson, D.I., Hilliou, L., 2014. Natural Giesekus: Shear and

768 Externsional Behavior of Food Gum Solutions in the Semidilute Regime. AIChE J. 60,
769 3902–3915.

770 Wang, Yu, Liu, J., Li, Q., Wang, Yitao, Wang, C., 2015. Two natural glucomannan polymers,
771 from Konjac and Bletilla, as bioactive materials for pharmaceutical applications. Biotechnol.
772 Lett. 37, 1–8.

773 Yoo, J.-W., Mitragotri, S., 2010. Polymer particles that switch shape in response to a stimulus.
774 Proc. Natl. Acad. Sci. 107, 11205–11210.

775 Zhu, F., 2018. Modifications of konjac glucomannan for diverse applications. Food Chem. 256,
776 419–426.

777

Figure 1

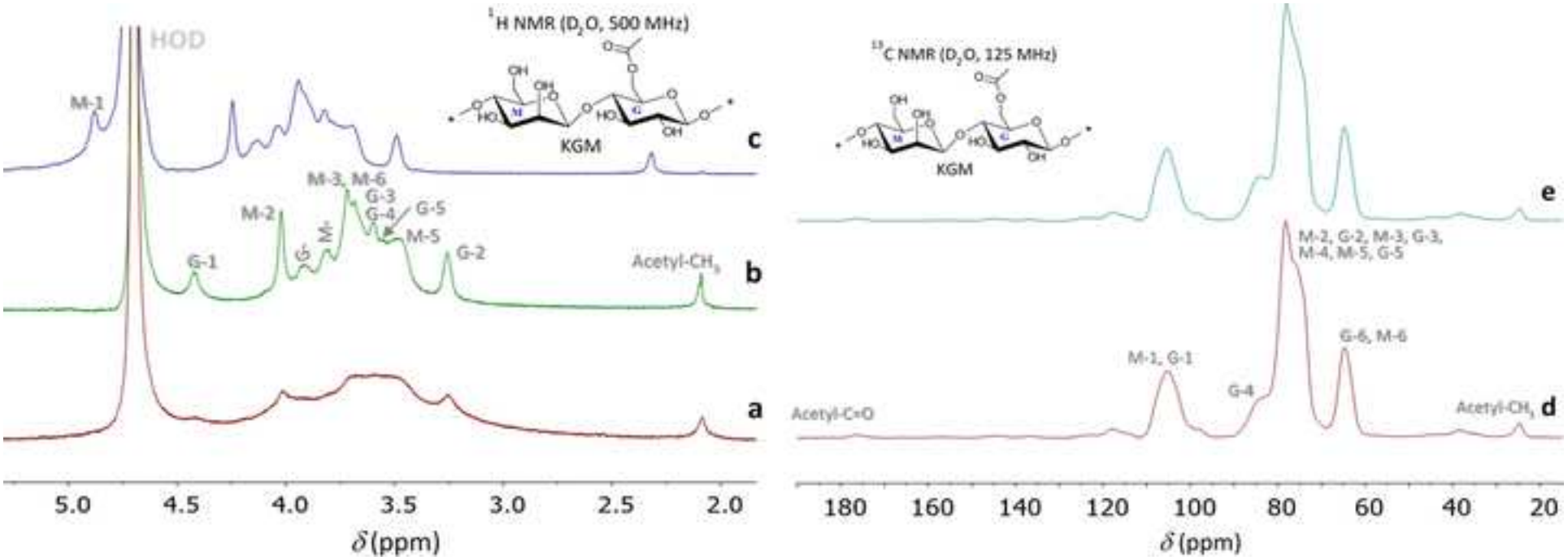

Figure 1.tif

Figure 2

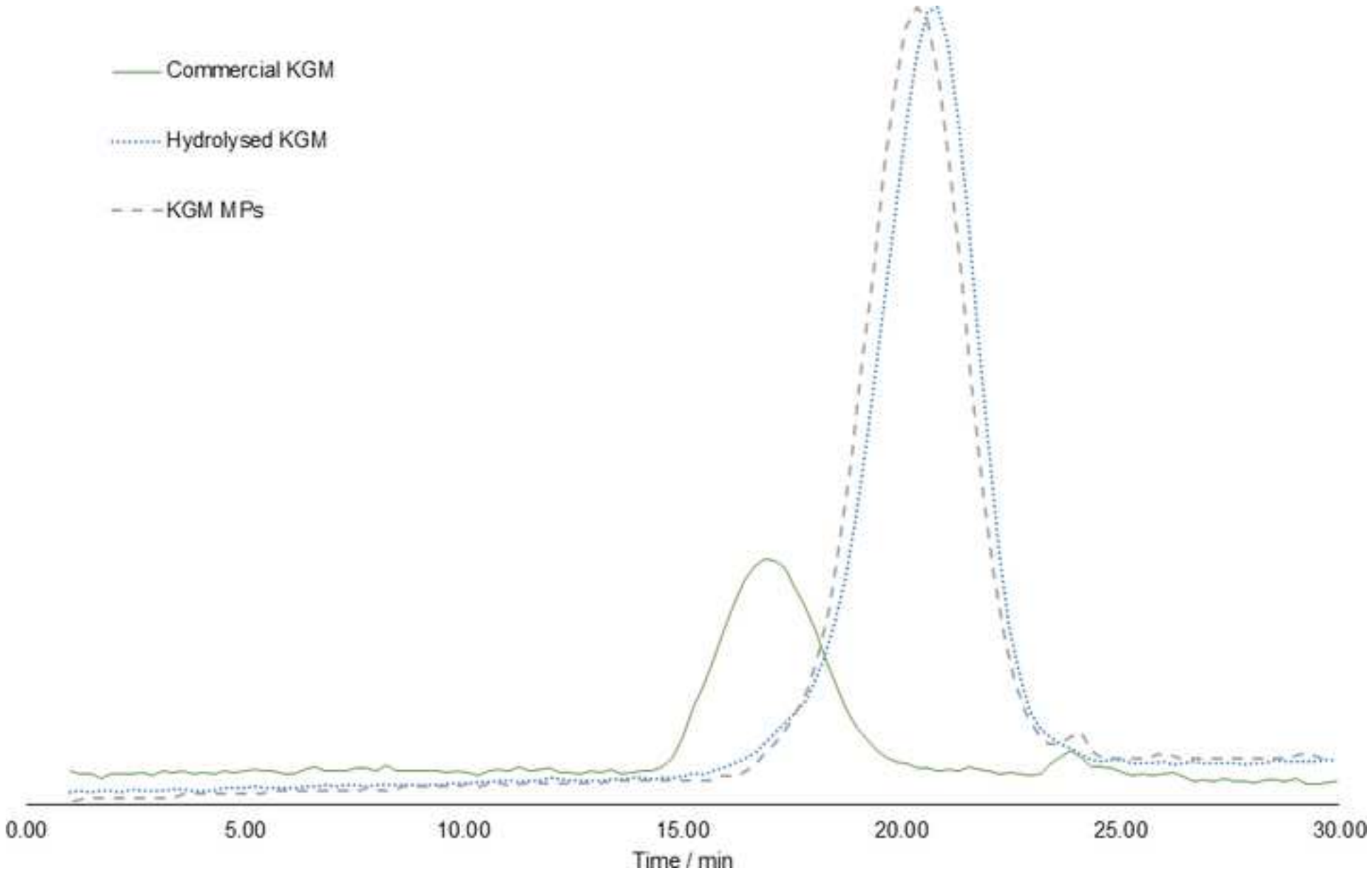

Figure 2.tif

Figure 3

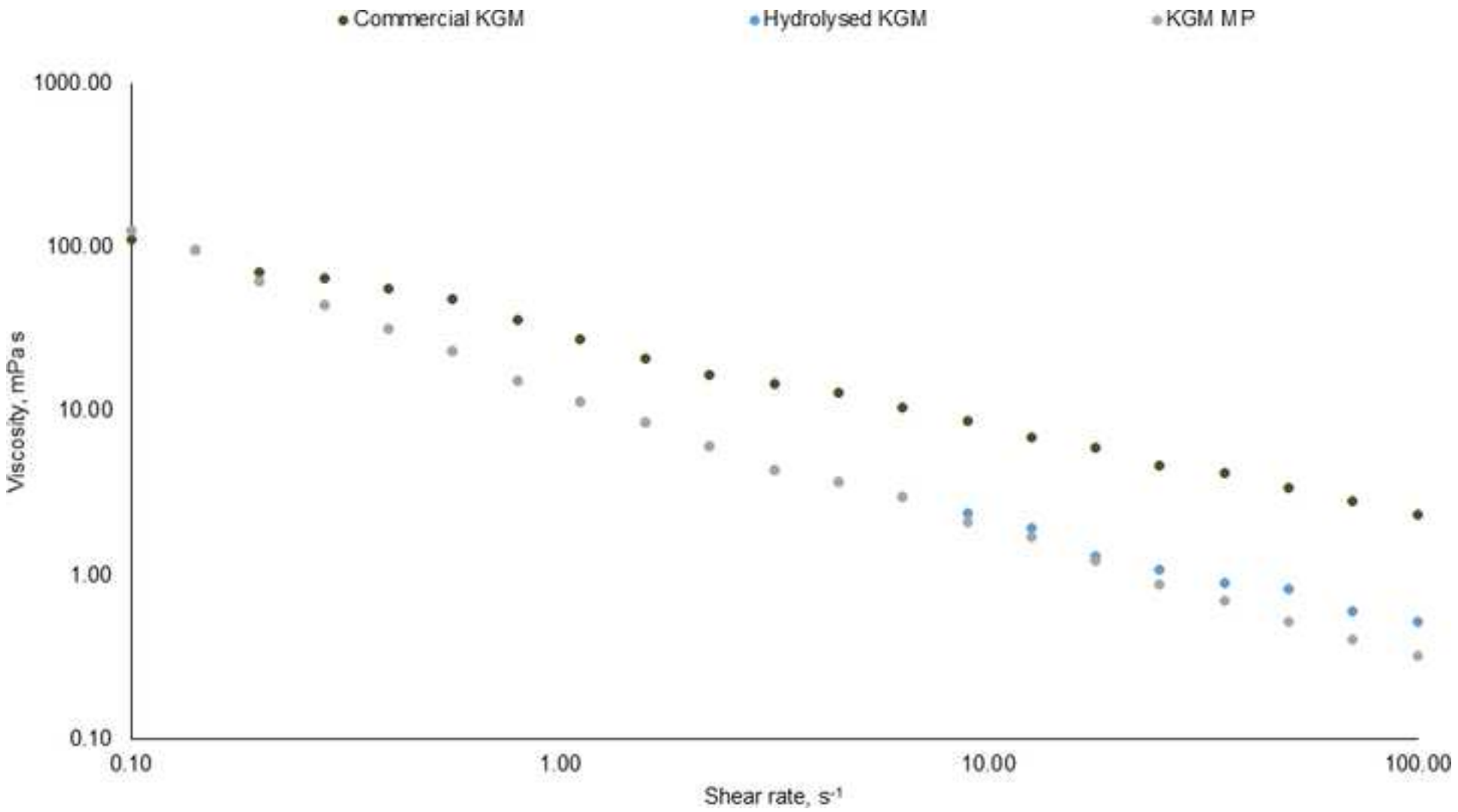

Figure 3.tif

Figure 4

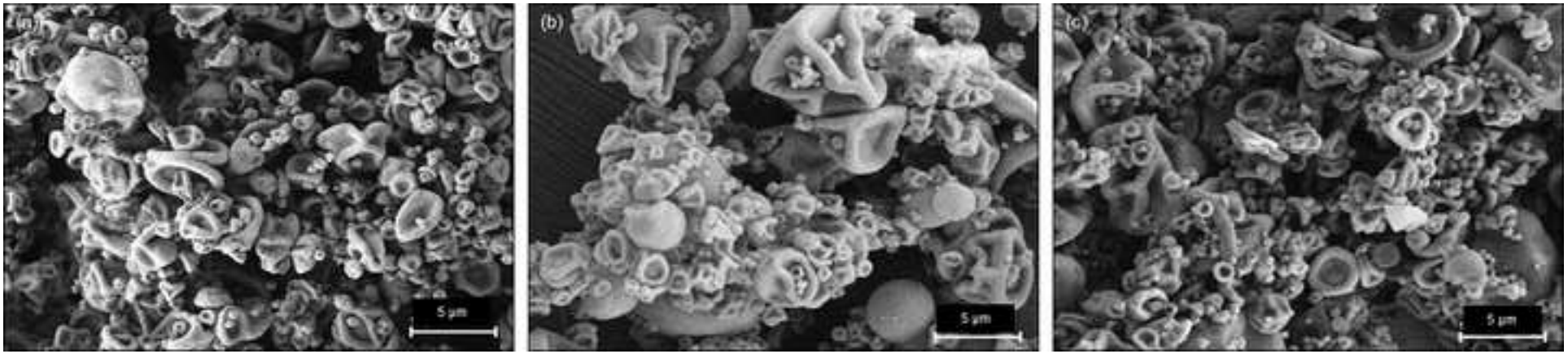

Figure 4.tif

Figure 5

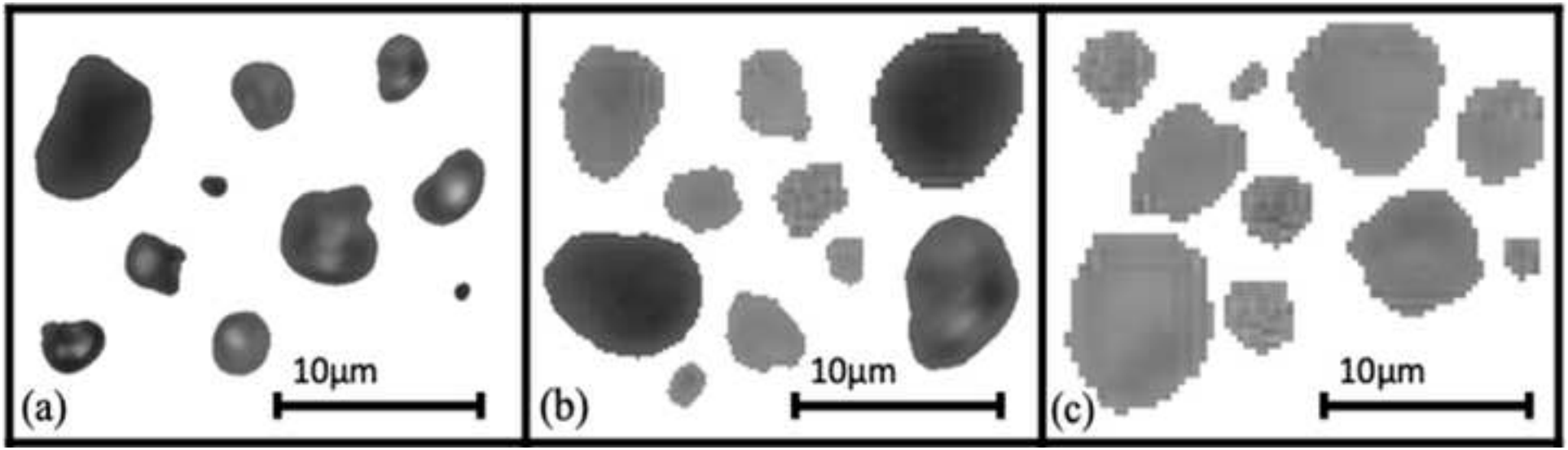

Figure 5.tif

Figure 6

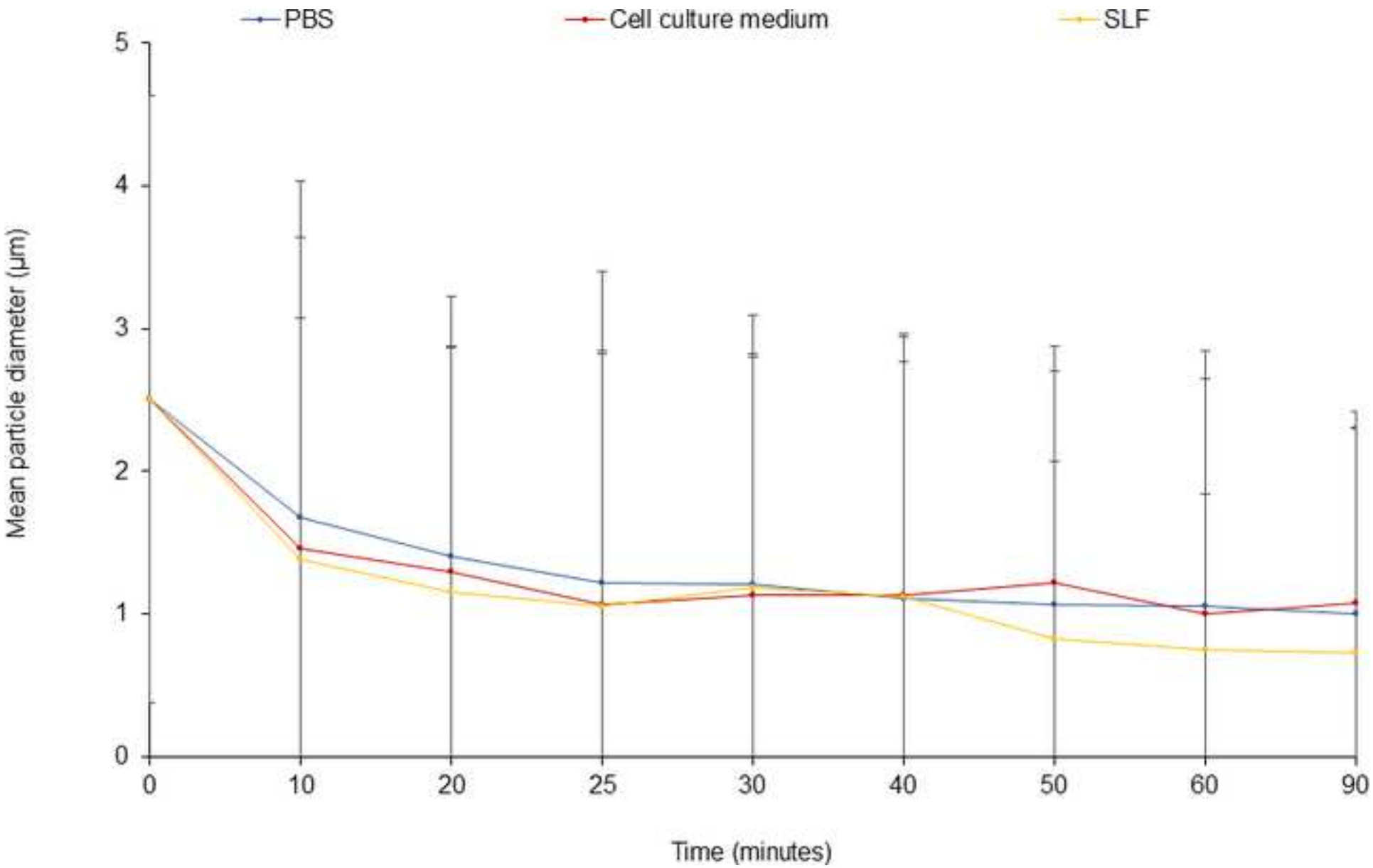

Figure 6.tif

Figure 7

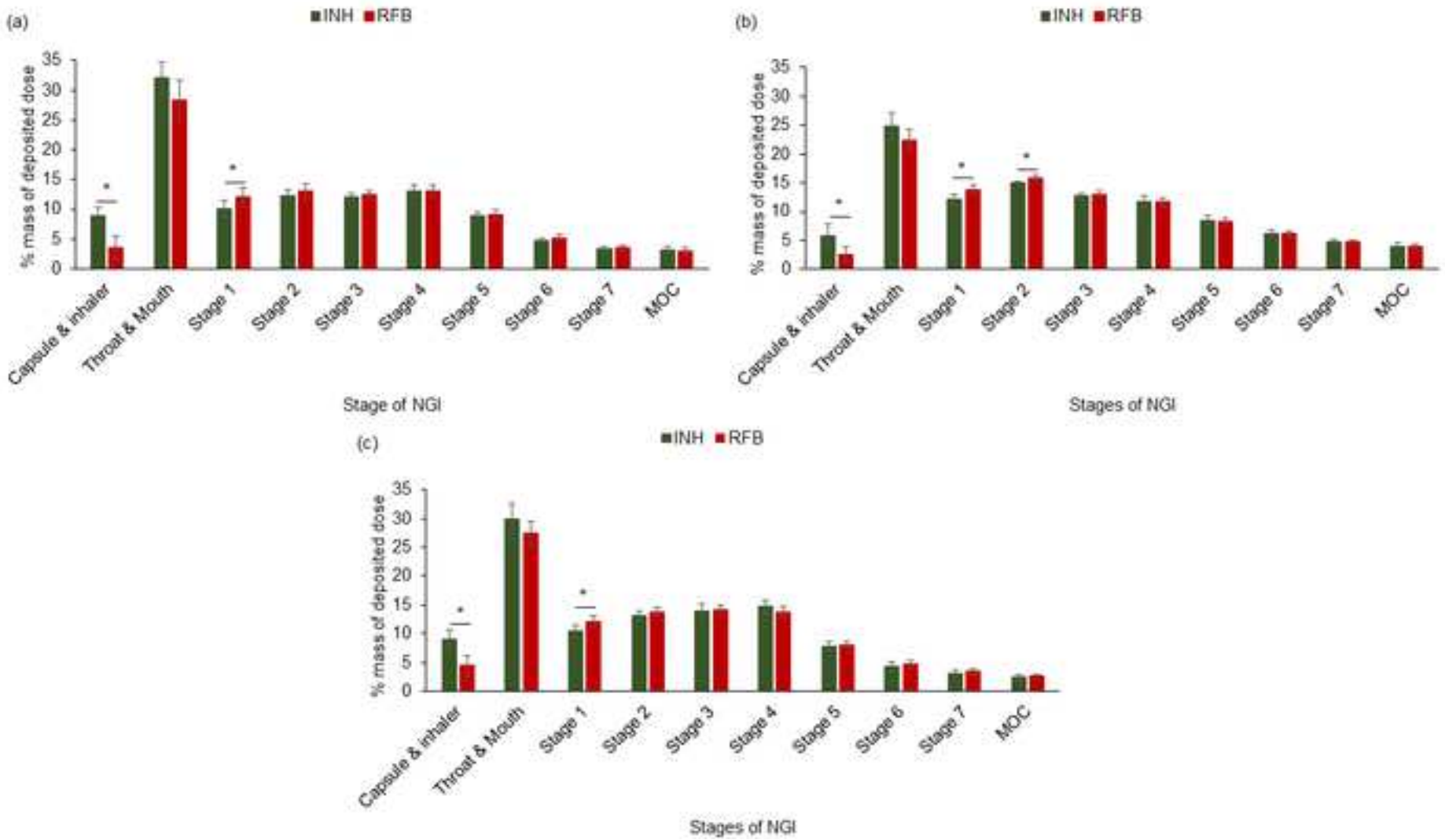

Figure 7.tif

Figure 8

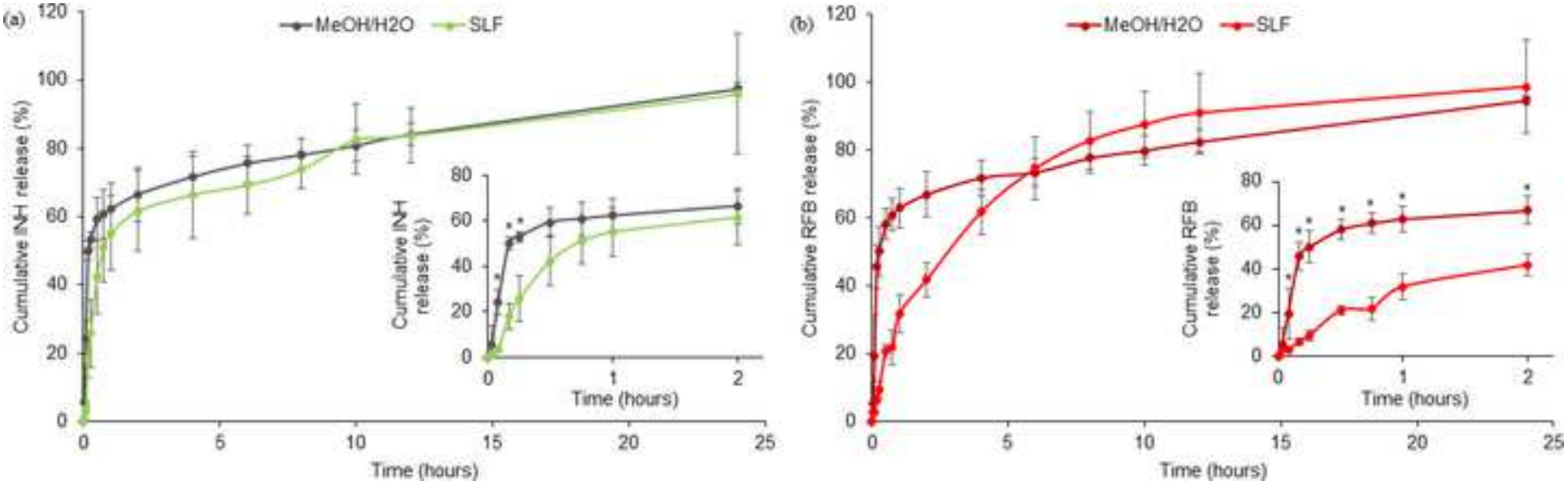

Figure 8.tif